buildings

MDPI

Article

Study on Construction Mechanical Characteristics and Offset Optimization of Double Side Drift Method for Large-Span Tunnels in Argillaceous Soft Rock

Wei He [1,2], Tengyu Wang [3,4,*], Yangyu Zhang [3,4] and Feng Wang [3,4]

[1] School of Highway Engineering, Chang'an University, Xi'an 710003, China
[2] Hubei Communications Investment Bachu Construction Management Co., Ltd., Enshi 444300, China
[3] Key Laboratory of Transportation Tunnel Engineering of the Ministry of Education, Southwest Jiaotong University, Chengdu 610031, China
[4] School of Civil Engineering, Southwest Jiaotong University, Chengdu 610031, China
* Correspondence: 2939409476@my.swjtu.edu.cn

Abstract

This study focuses on a large-span highway tunnel in argillaceous soft rock. Numerical simulations were conducted to investigate the mechanical characteristics of the tunnel, constructed using the Double Side Drift Method (DSDM), and the effects of the offset distance between drift faces. Subsequently, field monitoring was performed to analyze the deformation patterns of the primary support at typical cross-sections. The results indicate the following: (1) During DSDM construction in argillaceous soft rock, the crown settlement of the left drift is the largest, while that of the central drift is the smallest. The left and right drifts converge inward, whereas the central drift expands outward, resulting in overall inward convergence of the tunnel section, with the left drift exhibiting a larger convergence. The crown settlement and horizontal convergence induced by excavation of the upper benches of each drift are greater than those caused by the lower benches. (2) The stresses in the primary support increase rapidly after excavation of each segment and then tend to stabilize. The maximum tensile stress occurs at the left haunch, reaching 0.41 MPa, while the maximum compressive stress occurs at the left arch waist, reaching 14.56 MPa. After the tunnel excavation is completed and the section is enclosed, the stress on the left side is significantly higher than that on the right, indicating an eccentric stress state. The plastic zones in the surrounding rock exhibit a butterfly-shaped distribution, mainly concentrated at the haunches and arch springings on both sides. (3) As the offset distance decreases, the deformation of the primary support reduces, whereas the stress and the area of the surrounding rock plastic zones increase. When the offset distance is less than 15 m, both the stress in the primary support and the plastic zone area increase sharply, suggesting that the drift face offset distance should not be less than 15 m. (4) Field monitoring shows that the maximum cumulative crown settlement of the primary support reaches 30.2 mm, and the cumulative horizontal convergence of the section is 35.6 mm, both of which are below the reserved deformation allowance.

Keywords: argillaceous soft rock; large-span tunnel; Double Side Drift Method; construction mechanics; offset distance

Check for updates

Academic Editor: Eugeniusz Koda

Received: 3 November 2025
Revised: 25 November 2025
Accepted: 10 December 2025
Published: 20 December 2025

Copyright: © 2025 by the authors. Licensee MDPI, Basel, Switzerland. This article is an open access article distributed under the terms and conditions of the Creative Commons Attribution (CC BY) license.

1. Introduction

With the continuous growth of transportation demand in China, transportation infrastructure has been steadily expanded and improved. The construction of large-span

highway tunnels with single-bore three-lane or even four-lane configurations has become increasingly common [1–3]. However, due to their low flat ratio and complex construction procedures, the mechanical behavior during construction is highly complicated, particularly in soft rock formations. As a result, actual construction often faces dual challenges in terms of schedule and safety.

Nowadays, numerous studies have investigated the mechanical behavior of large-section tunnels during construction, with research efforts mainly focusing on cases where tunnels are located in soil layers [4–11] or moderately weathered hard rock formations [12–21]. In contrast, specialized studies on large-span tunnels in mudstone soft rock or other weathered soft rock formations remain relatively limited. Tao [22] conducted numerical analyses on an extremely large-section tunnel excavated using the central diaphragm method in moderately weathered mudstone, and reported that the plastic zone of the surrounding rock mainly develops around the haunches and arch springings, dominated by shear failure. Lin [23] investigated the mechanical behavior of tunnels constructed using the DSDM and the central diaphragm method in mudstone soft rock through a combination of numerical simulation and field monitoring. Tan [24], based on laboratory geomechanical testing and numerical simulation, examined the deformation patterns of the support system in mudstone tunnels and performed parameter analyses to determine key construction parameters such as the thickness of shotcrete and the installation timing of the secondary lining.

For large-section tunnels, the full-face excavation is typically divided into multiple segments, and the longitudinal staggered distance between excavation faces plays a critical role in the deformation and stress distribution within the support system. Several researchers have investigated the reasonable staggered distance between excavation faces in such multi-stage excavation schemes. Jiang [25], based on a metro tunnel project adopting DSDM, determined the optimal staggered distances between the left, right, and central drifts through numerical simulation. Wang [26], using the Xiamen Xiang'an Highway Tunnel as a case study, proposed the optimal spacing between drifts based on numerical simulation combined with construction requirements. Wang [27] proposed an improved central diaphragm method for a large-span soft rock tunnel and investigated the optimal staggered distance between drifts through numerical analysis and field monitoring.

In summary, current studies on large-span tunnels have mainly focused on the mechanical behavior associated with the application of DSDM or the central diaphragm method in weak soil layers or moderately weathered granite or limestone formations, whereas research specifically addressing the use of DSDM in soft rock formations remains insufficient. Moreover, the reasonable staggered distance between working faces in soft rock has not yet been clearly established. To address this gap, this study focuses on a large-span highway tunnel in mudstone soft rock and investigates the mechanical characteristics of DSDM through numerical simulation and field monitoring. In addition, the staggered distance between working faces is optimized to provide practical guidance for the design and construction of large-span tunnels in mudstone soft rock.

2. Project Background

2.1. Project Overview

A separated single-tube, four-lane highway tunnel is planned to be constructed in the southwest region of China. The tunnel has a total design length of 2168 m, with a design speed of 80 km/h and a maximum overburden depth of approximately 135 m. The excavation span reaches 21 m, while the tunnel cross-section has a height of 13.69 m and a width of 20.94 m, resulting in an excavation area of approximately 210 m^2.

The strata at the tunnel site exhibit a monoclinal structure, with an overall dip direction of approximately 300° and dip angles ranging from 25° to 40°. The tunnel mainly passes through moderately weathered mudstone with a natural uniaxial compressive strength of 4.25–7.23 MPa, which is classified as soft rock. This type of rock is prone to disintegration upon water exposure, characterized by well-developed joints and fissures, highly fractured structure, and poor self-stability.

According to the Chinese specification Specifications for Design of Highway Tunnels (JTG 3370.1-2018) [28], the surrounding rock of the tunnel is classified as Grade V. Under this rock condition, construction design requires that the cumulative tunnel crown settlement and horizontal convergence must not exceed 50 mm. In addition, the deformation control limit specified in the Chinese code Specifications for Design of Highway Tunnels (JTG 3370.1-2018) [28] is 150 mm. The tunnel excavation was carried out using the drill-and-blast method.

The highway tunnel adopts a composite lining system, in which the primary support mainly consists of steel arch frames and shotcrete, while the secondary lining is constructed using reinforced concrete. The detailed geometric dimensions of the tunnel and the surrounding geological conditions are shown in Figure 1.

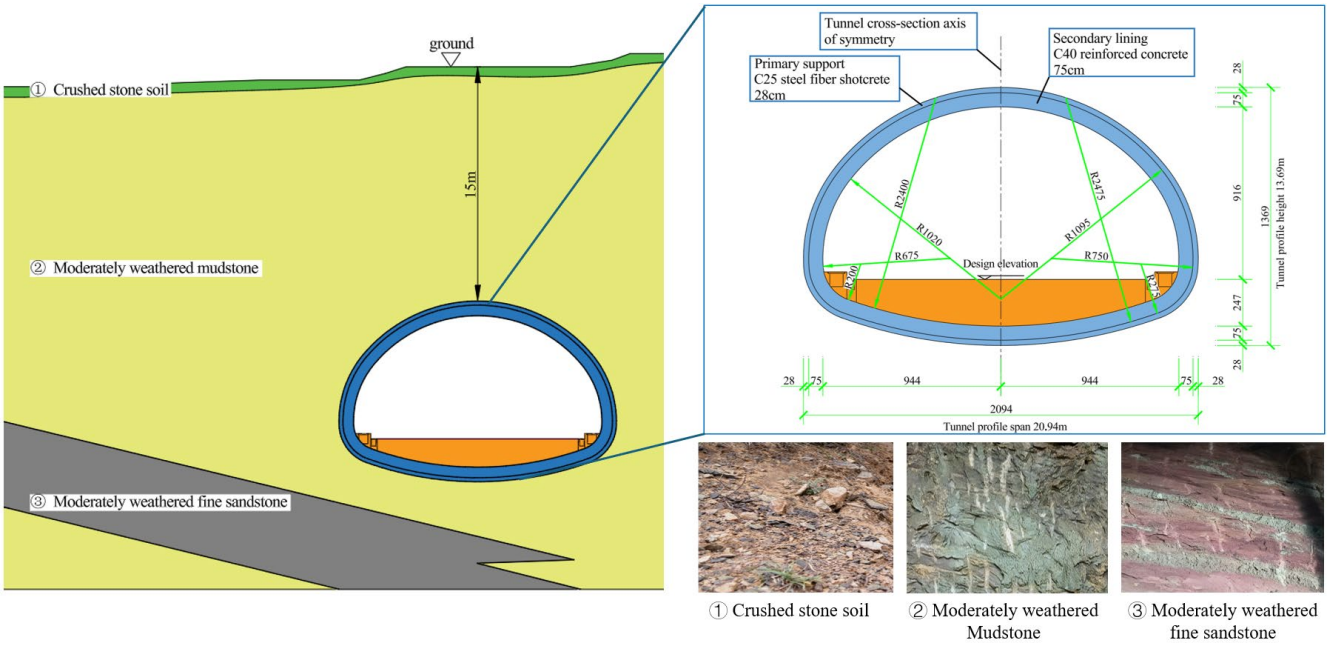

Figure 1. Surrounding geology and tunnel structure.

2.2. Construction Method and Sequence for Large-Span Tunnel in Argillaceous Soft Rock

2.2.1. Construction Parameters of Each Structure

According to the design documents, the tunnel adopts a composite lining system, in which the primary support consists of steel arch frames and shotcrete, the secondary lining is constructed of reinforced concrete, and the temporary support is composed of steel arch frames and shotcrete. The primary support, serving as the permanent load-bearing structure, adopts HW200 × 200 wide-flange H-sections with relatively high stiffness. The temporary supports, which are removed after the primary support forms a closed ring, utilize I20b I-sections with comparatively lower stiffness. Connections between the HW200 × 200 I-beams of the primary support are achieved through bolted and welded joints, whereas the I20b I-beams used for the temporary support, as well as their connections with the HW200 × 200 I-beams of the primary support, are joined using easily removable bolted

connections. The construction parameters of each structural component are summarized in Table 1.

Table 1. Construction parameters of each tunnel structure.

Structure	Material	Parameters
primary support	steel arch frame shotcrete	HW200 × 200 steel frame, with a spacing of 50 cm between each frame Strength grade C25, thickness 0.28 m
temporary support	steel arch frame shotcrete	I20b I-steel, with a spacing of 50 cm Strength Grade C25, Thickness 22 cm
secondary lining	reinforced concrete	Strength Grade C40, Thickness 75 cm

2.2.2. Tunnel Construction Methods and Sequences

Considering the large excavation span and poor surrounding rock quality of the proposed tunnel, the DSDM is planned for construction. Each excavation cycle advances by 0.5 m, consistent with the spacing of the steel arch frames. The length of each bench in the drifts is 5 m, and the staggered distance between the upper bench faces of each drift is uniformly controlled at 15 m. The detailed construction sequence is illustrated in Figure 2 and summarized in Table 2.

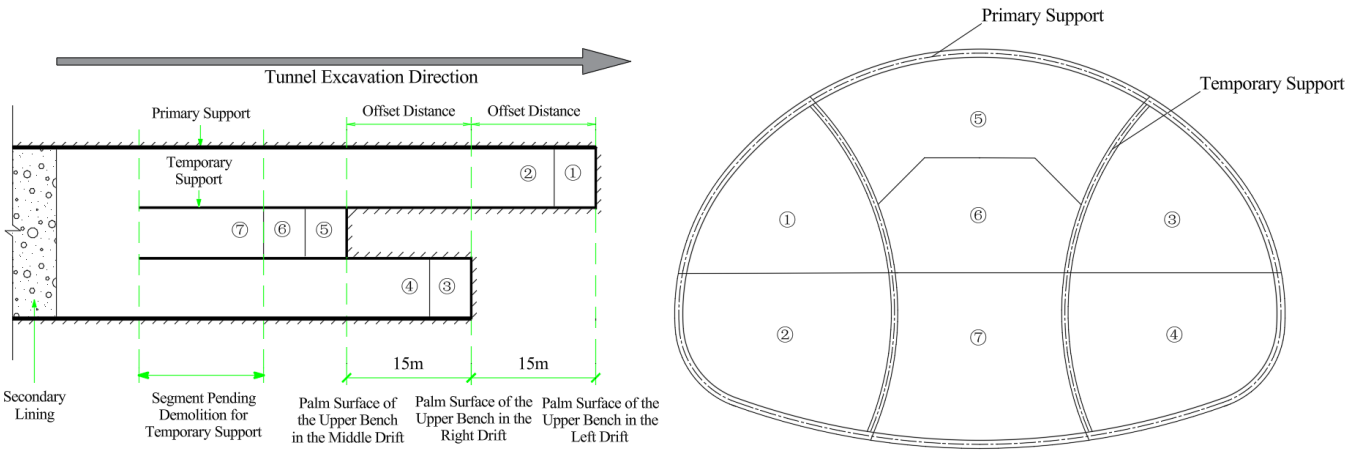

(**a**) (**b**)

Figure 2. Schematic illustration of the DSDM: ((**a**) plan view of the construction layout; (**b**) cross-sectional division of the tunnel).

Table 2. Tunnel construction sequence.

Construction Steps	Construction Operations *
1	Excavate Part ①, and construct the primary support and temporary support for the upper bench of the left drift
2	Excavate Part ②, and construct the primary support and temporary support for the lower bench of the left drift
3	Excavate Part ③, and construct the primary support and temporary support for the upper bench of the right drift
4	Excavate Part ④, and construct the primary support and temporary support for the lower bench of the right drift
5	Excavate Part ⑤, and construct the primary support
6	Excavate Part ⑥
7	Excavate Part ⑦, and enclose the primary support to form a ring
8	Remove the Temporary Support
9	Construct the Tunnel Secondary Lining

* The sequence numbers of the excavation stages in the table correspond directly to those shown in Figure 2.

3. Numerical Model

3.1. Establishment of the Numerical Model

In this study, numerical simulations of the Double Side Drift Method (DSDM) construction process for a large-span tunnel in mudstone soft rock were performed using FLAC3D 6.0 software. The section from chainage ZK13 + 400 to ZK13 + 460 was selected as the study segment, and a three-dimensional numerical model was established (see Figure 3). The tunnel overburden depth in this segment is 15 m, and the excavation direction is parallel to the positive Y-axis of the model. The model dimensions are 160 m × 60 m × 89 m (X × Y × Z). In the horizontal direction (X-axis), the model width is set to four times the tunnel excavation diameter; the distance from the tunnel invert to the model bottom boundary is four times the tunnel excavation height; and the distance from the tunnel crown to the model top boundary is 15 m. For meshing, a 2D planar grid was first created in MIDAS GTX NX 2019 software on planes perpendicular to the excavation direction, which was then extruded along the tunnel excavation direction to generate the full 3D mesh [29]. The mesh was subsequently exported as a FLAC3D-readable file. In the numerical model, the primary support and temporary support were modeled using shell elements, while the surrounding rock mass and the secondary lining were modeled using zone elements, with a minimum size of 0.5 m and a maximum size of 3 m. The model consists of a total of 529,320 elements and 546,073 nodes. Normal constraints were applied to the four lateral boundaries and the bottom boundary, while the top boundary was set as a free boundary. During the simulation of the tunneling process, gravity loading was first applied to the entire model. After obtaining the initial geostress field, the model displacements were reset to zero. Subsequently, the excavation cycles were controlled using the built-in FISH programming language in FLAC3D (FISH is the built-in scripting language specific to FLAC3D. The name "FISH" is conventionally retained in the industry and is usually referred to as the "FISH programming language." It is primarily used to customize numerical computation logic), with each excavation cycle advancing 0.5 m, until the tunnel was fully excavated.

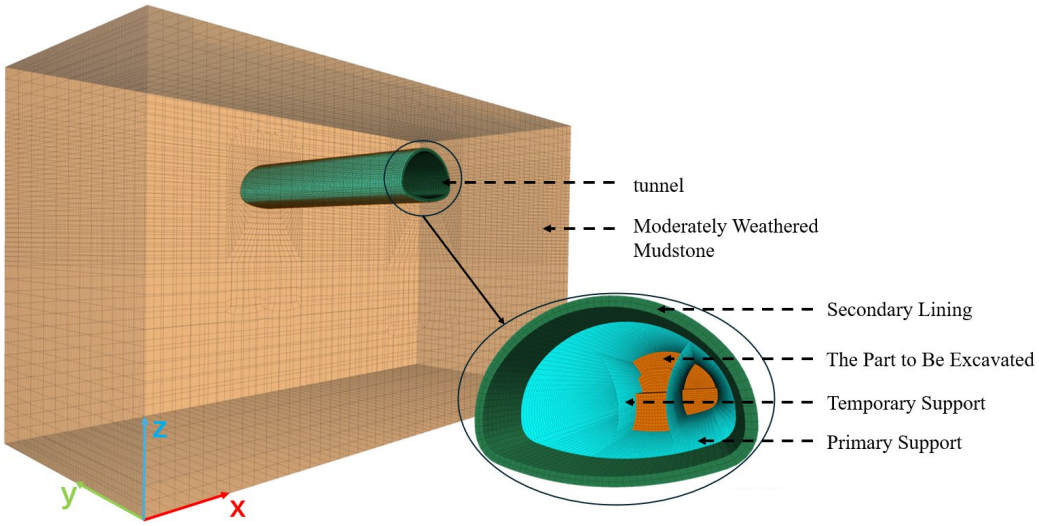

Figure 3. Numerical calculation model.

3.2. Model Assumptions and Parameter Settings

In actual engineering practice, the rock and soil mass within the influence zone of tunnel excavation is often a heterogeneous, anisotropic, and nonlinear material. It is difficult to represent the mechanical behavior of the ground during tunnel construction using a single constitutive model in numerical simulations. To simplify the model, the following assumptions were made in this study: 1. The rock mass is considered a homogeneous, con-

tinuous, isotropic elastoplastic material conforming to the Mohr–Coulomb yield criterion; 2. The tunnel primary support, temporary support, and secondary lining are modeled as isotropic linear elastic materials; 3. In accordance with the Specifications for Design of Highway Tunnels (JTG 3370.1-2018) [28], the stress-sharing ratios among the surrounding rock and support structures are set as follows: the surrounding rock bears 30%, the primary support bears 40%, and the secondary lining bears 30% of the load; 4. The creep behavior of moderately weathered mudstone is not considered in the model; 5. The construction time of each excavation step is not considered, and the effects induced by each construction step are treated as a quasi-static process; 6. Using the equivalent stiffness method expressed in Equation (1) [30–32], the elastic moduli of steel arch frames, reinforcement, and other components in the tunnel support system are converted to corresponding values for the lining structure.

The physical and mechanical parameters of the surrounding rock and support structures were determined based on the design documents, geological survey data of the project, and Specifications for Design of Highway Tunnels (JTG 3370.1-2018) [28]. Table 3 summarizes the physical and mechanical parameters of the various materials used in the model.

$$E = E_c + E_a \frac{S_a}{S_c} + E_m \frac{S_m}{S_c} \quad (1)$$

where E is the equivalent elastic modulus of the support structure; E_c is the elastic modulus of the shotcrete; E_a and S_a are the elastic modulus and cross-sectional area of the steel arch frame, respectively; and E_m and S_m are the elastic modulus and cross-sectional area of the reinforcement, respectively.

Table 3. Table of physical and mechanical parameters of the model.

Material Type	Density /(kg m^{-3})	Elastic Modulus /GPa	Poisson's Ratio	Cohesion /MPa	Internal Friction Angle /°	Thickness /m
Moderately Weathered Mudstone	2300	1.1	0.34	0.2	23	/
Secondary Lining	2400	34.2	0.2	/	/	0.75
Primary Support	2300	32	0.2	/	/	0.28
Temporary Support	2300	30	0.2	/	/	0.22

4. Results and Discussion

4.1. Mechanical Characteristics of DSDM Construction for Large-Span Tunnels in Argillaceous Soft Rock

To reduce the impact of boundary effects, the middle part of the model (i.e., the cross-section at the excavation position Y = 30m) was selected as the research object. Measuring points were arranged according to the positions shown in Figure 4 to conduct an in-depth analysis of the variation laws of primary support deformation, stress, and surrounding rock plastic zone during the construction of the large-span argillaceous soft rock tunnel using the DSDM.

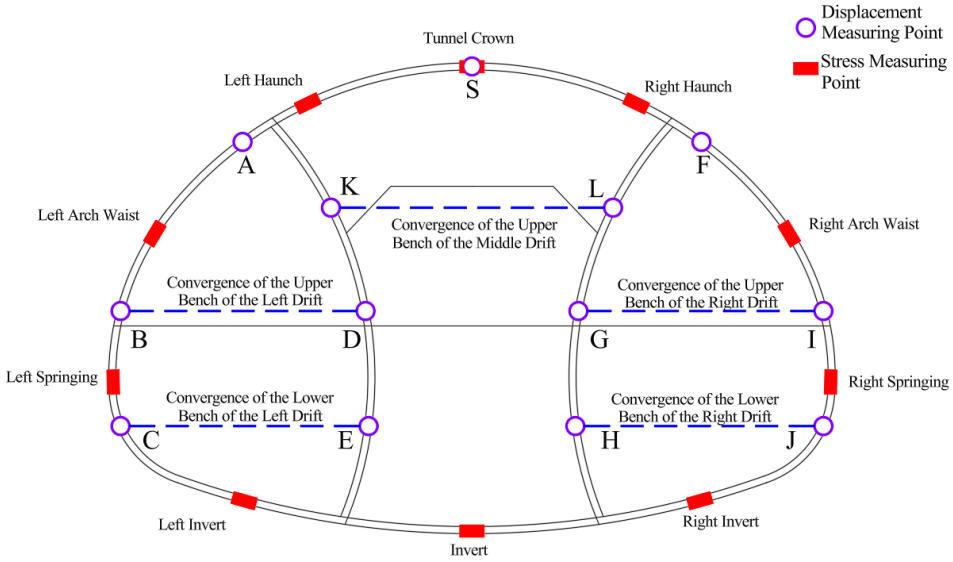

Figure 4. Layout diagram of measuring points on the numerical simulation cross-section. (horizontal convergence is defined as positive for inward convergence and negative for outward expansion).

4.1.1. Analysis of Primary Support Deformation

Figure 5 presents the time-history curves of tunnel crown settlement during excavation. As shown in Figure 5, the maximum tunnel crown settlement occurs in the left drift, with a cumulative value of 28.4 mm. The crown settlements in the central and right drifts are comparatively smaller, with the right drift reaching a cumulative settlement of 22.2 mm, and the central drift exhibiting the smallest cumulative settlement of only 20.5 mm. Since the upper bench of the left drift is excavated earlier than the other drifts, and the subsequent excavation of other segments imposes significant disturbance on the surrounding rock at the left drift, its deformation is further amplified. Consequently, the final cumulative crown settlement of the left drift is significantly larger than that of the other drifts.

The crown settlement of the primary support in each drift increases rapidly after the corresponding upper bench excavation is completed, and then gradually slows down as subsequent excavation progresses. After the temporary support is removed, the crown settlement of the primary support gradually stabilizes. Taking the left drift crown settlement as an example, the excavation of the upper bench of the left drift (Part ①) induces the largest crown settlement, accounting for 28% of the total settlement. The excavation of the right drift has a relatively minor impact. After the upper bench of the central drift (Part ⑤) is excavated, a noticeable secondary increase in the crown settlement of the left drift is observed, contributing approximately 17.5% of the total settlement. This is because the upper bench of the central drift is adjacent to the left drift, and its excavation generates significant disturbance in the surrounding rock of the left drift, leading to stress redistribution and further deformation of the primary support. Since the primary support forms a closed ring after the excavation and installation of the tunnel invert support, the overall deformation of the primary support gradually stabilizes, and the removal of temporary support has a minimal effect.

Figure 6 presents the time-history curves of horizontal convergence for each drift during tunnel excavation. In this study, inward convergence is defined as positive, and outward expansion as negative. As shown in Figure 6, when the DSDM is applied, the left and right drifts converge inward, with the upper bench of the left drift exhibiting the largest convergence of 31.8 mm, and the upper bench of the right drift reaching 28.5 mm, while the central drift experiences a cumulative outward expansion of 29.8 mm. The horizontal convergence of the lower benches in the left and right drifts is slightly smaller than that

of the upper benches, with the left drift lower bench converging by 23.6 mm, 8.2 mm less than the upper bench, and the right drift lower bench converging by 18.27 mm, 10.23 mm less than the upper bench.

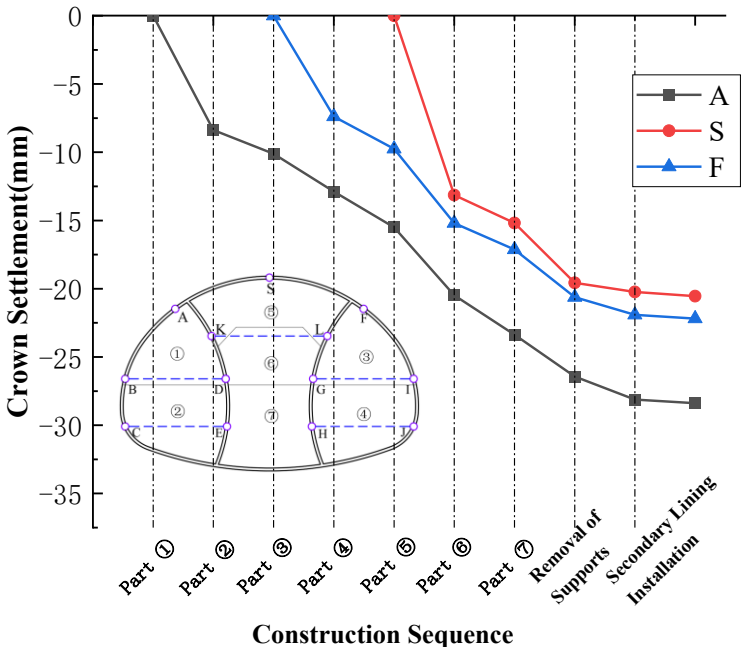

Figure 5. Crown settlement of each drift.

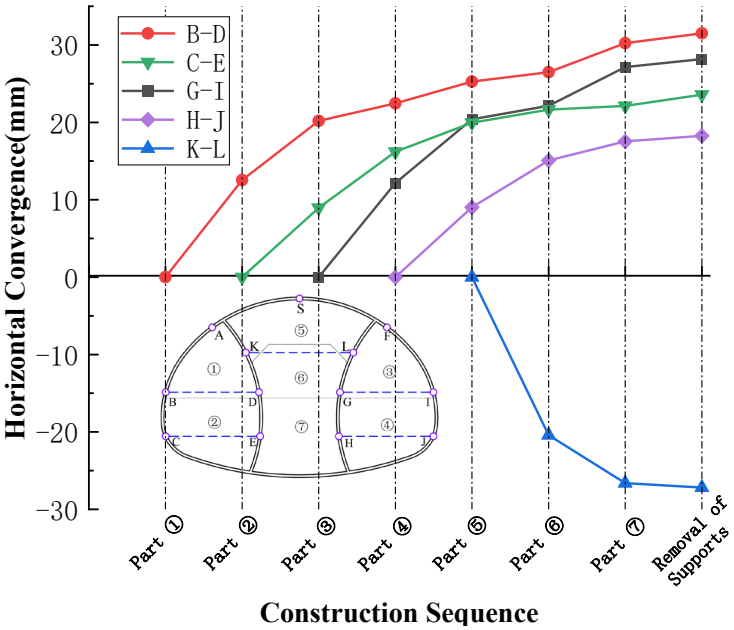

Figure 6. Horizontal convergence of each drift.

The development pattern of horizontal convergence in the primary support is generally similar for all drifts. After each excavation segment, the convergence increases sharply, then the growth rate gradually decreases, and finally stabilizes before the temporary support is removed. The excavation of the upper benches has the greatest influence on horizontal convergence. Taking the left drift upper bench as an example, the excavation of the upper bench of the left drift (Part ①) accounts for 39.8% of the final cumulative convergence. The excavation of the lower bench of the left drift (Part ②) has a relatively minor effect, contributing approximately 24.4% of the horizontal convergence. Following the excavation

of the central drift, the growth rate of horizontal convergence in the left drift slightly decreases and then gradually stabilizes.

4.1.2. Analysis of Primary Support Force

Figure 7 presents the time-history curves of the maximum and minimum principal stresses at various measurement points of the primary support. As shown in Figure 7a, the overall tensile stress in the tunnel primary support is relatively small, whereas the tensile stresses at the left and right haunches, left and right arch waists, and left arch springing are significantly higher than at other locations. Among these, the maximum tensile stress occurs at the left haunch, reaching 0.41 MPa, while the tensile stress at the tunnel crown is the lowest, only 0.01 MPa. After excavation, the tensile stress at each measurement point in the primary support increases rapidly and then gradually stabilizes. Following the excavation of the upper bench of the central drift (Part ⑤), a pronounced secondary increase in tensile stress occurs at the haunches and arch waists on both sides of the tunnel. This is because, after the excavation and installation of primary support in the upper bench of the central drift, the upper portion of the primary support forms a continuous structure that collectively bears the load, resulting in substantial surrounding rock pressure and rapid growth of tensile stress at the haunches and arch waists. After the removal of temporary support, the tensile stress at the left and right arch waists decreases noticeably and eventually stabilizes. It can be inferred that during DSDM construction, the connections between temporary support and primary support are prone to tensile stress concentration, which is alleviated after the removal of temporary support, leading to a significant reduction in tensile stress at the haunches.

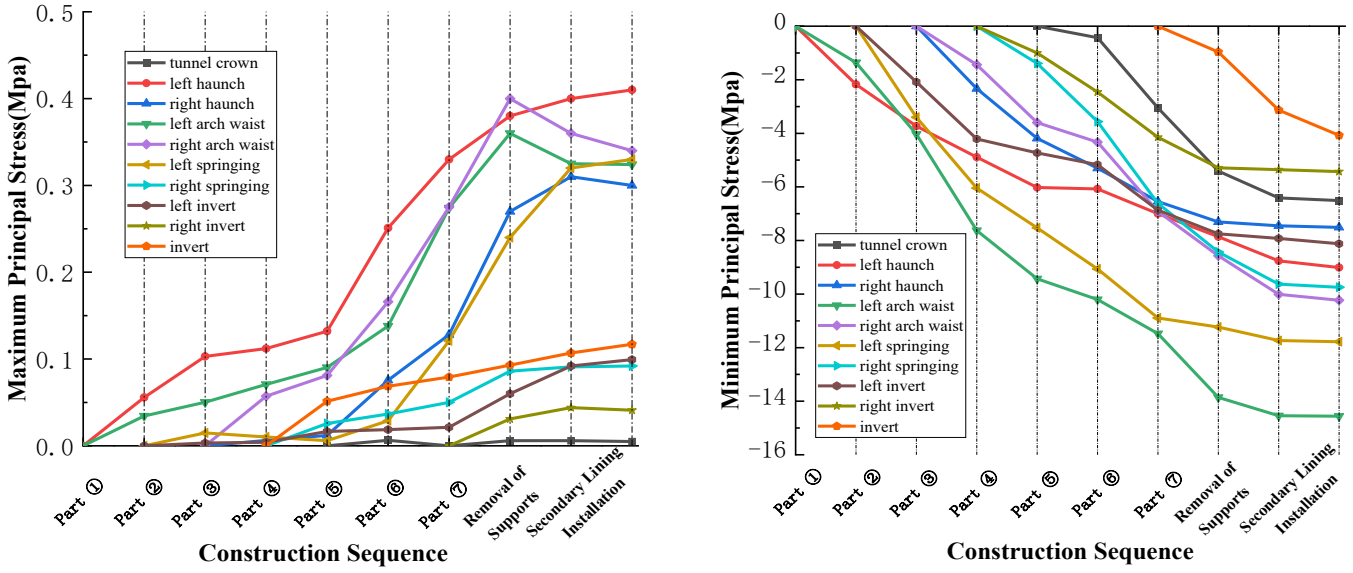

Figure 7. Diagram of principal stress changes in primary support ((**a**) Maximum Principal Stress; (**b**) Minimum Principal Stress).

As shown in Figure 7b, the compressive stress is relatively large at the arch waists and arch springings, with the maximum compressive stress of 14.56 MPa occurring at the left arch waist, and the minimum compressive stress of 4.07 MPa at the tunnel invert. After each excavation segment, the compressive stress in the primary support increases rapidly, then the growth rate gradually decreases, and finally stabilizes after the temporary support is removed. Upon completion of the overall tunnel excavation, the compressive stress in the left primary support is significantly higher than that on the right. This is because the

left drift is excavated first, and the surrounding rock in this region has already undergone plastic deformation. During the subsequent excavation of other segments, the plastic zone around the left drift further develops due to disturbances from the later excavations, resulting in a rapid increase in surrounding rock pressure on the left side and placing the tunnel under asymmetric stress conditions.

4.1.3. Development Law of Plastic Zone

Figure 8 illustrates the development of the plastic zones during the tunnel excavation process. As shown in the figure, after the upper bench of the left drift is excavated, the plastic zones are mainly concentrated in the lower bench of the left drift and in the middle drift. Once the upper bench of the right drift is completed, the rock pillar in the middle drift undergoes overall shear failure. After the lower bench of the right drift is excavated, the plastic zones at the arch springings on both sides of the tunnel begin to expand. With the continued excavation of the middle drift, the plastic zones at the haunches and arch springings on both sides rapidly develop, and a slight expansion of the plastic zone at the haunches occurs after the removal of the temporary support. When the overall tunnel excavation is completed, the plastic zones exhibit a butterfly-shaped distribution, mainly concentrated at the haunches and arch springings on both sides of the tunnel. The main reason for the butterfly-shaped distribution of the plastic zone is that, during tunnel excavation in soft rock using the DSDM, the left and right drifts are excavated prior to the central drift. Following the excavation of the side drifts, the rock mass at the drift crowns (corresponding to the tunnel haunches) undergoes settlement deformation and develops plastic zones, which continue to expand under excavation-induced disturbance. After the upper bench of the central drift is excavated, the supporting structures become interconnected, forming a complete arch. At this stage, the load transferred from the surrounding rock above the arch is transmitted along the arch to the arch springings on both sides, and subsequently to the surrounding rock in these regions, leading to the development of plastic zones near the arch springings. As a result, the plastic deformation becomes concentrated at the haunches and arch springings on both sides of the tunnel, ultimately forming a butterfly-shaped plastic zone distribution. Therefore, in practical construction, monitoring of the haunch and arch springing areas should be enhanced, and reinforcement measures should be implemented when necessary.

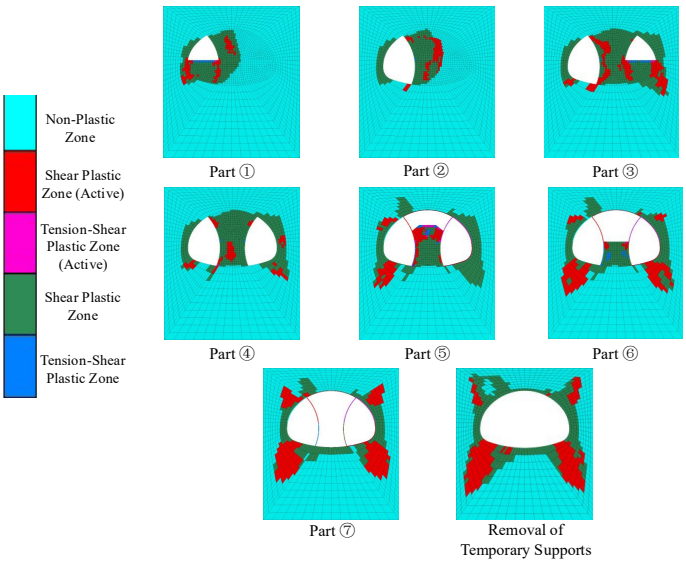

Figure 8. Development of tunnel plastic zone.

4.2. Influence of Face Offset Between Drifts on DSDM Excavation

During segmented excavation of large-span tunnels in soft rock, the offset distance between the drift faces (i.e., the distance between the drift faces, as indicated by the "offset distance" in Figure 2) is a critical factor influencing the stress and deformation of the support system. When the offset distance between drift faces is too short, the primary support installed in the preceding drift has not yet stabilized, and subsequent excavation induces significant disturbance in the surrounding rock, increasing the load on the support structure. Moreover, excessively short offset distances are unfavorable for the transition between construction sequences in large-span tunnels. Conversely, when the offset distance between drifts is too long, the primary support remains unclosed for extended periods, which adversely affects the stability of stress and deformation in the support, and also significantly reduces construction efficiency.

Therefore, this study investigates the offset distance between drifts during DSDM construction of a large-span tunnel in mudstone soft rock. Five scenarios were considered, with the offset distances of the left drifts set to 5 m, 10 m, 15 m, 20 m, and 25 m, respectively. The influence of different offset distances on the deformation and stress of the tunnel primary support, as well as on the development of the surrounding rock plastic zones, was analyzed in detail to determine an optimal offset distance.

4.2.1. Deformation Analysis of the Primary Support

Figure 9 shows the variation in primary support deformation with the offset distance between drift faces after tunnel excavation. As shown in the figure, the tunnel crown settlement decreases linearly with decreasing offset distance. When the offset distance is 25 m, the crown settlement of the primary support is 21.6 mm. As the offset distance is reduced to 20 m, 15 m, 10 m, and 5 m, the crown settlement decreases by 0.51 mm, 0.69 mm, 0.47 mm, and 0.62 mm, corresponding to reductions of 2.4%, 3.2%, 2.2%, and 2.9%, respectively.

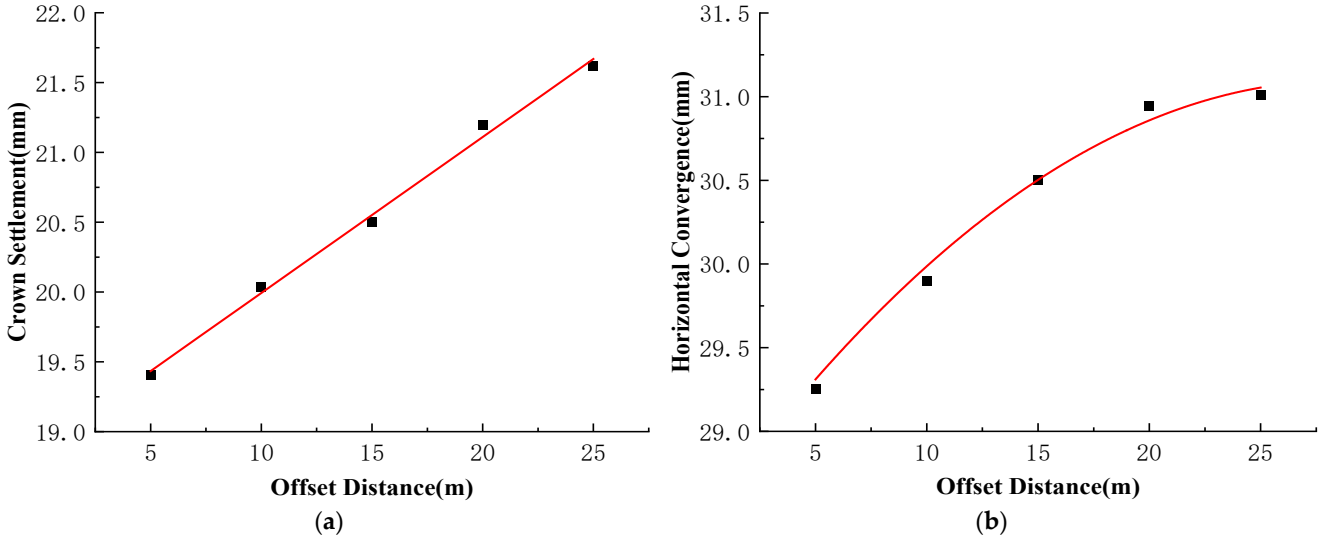

Figure 9. Deformation laws of primary support with different offsets ((**a**) Crown Settlement of Primary Support; (**b**) Horizontal Convergence of Primary Support).

The tunnel horizontal convergence also decreases with decreasing offset distance, following a parabolic trend. When the offset distance is 25 m, the horizontal convergence of the primary support is 31.1 mm. As the offset distance decreases to 20 m and 15 m, the horizontal convergence becomes 30.9 mm and 30.5 mm, corresponding to reductions of 0.6% and 1.3%, respectively. When the offset distance is further reduced to 10 m and 5 m,

the horizontal convergence decreases sharply to 29.9 mm and 29.1 mm, with reductions of 1.9% and 2.6%, respectively. This behavior is attributed to the earlier closure of the drifts into a continuous ring with decreasing offset distance, which is more favorable for controlling the deformation of the primary support.

4.2.2. Stress Analysis of the Primary Support

Figure 10 presents the variation in the maximum tensile and compressive stresses in the primary support with the offset distance between drift faces. As shown in Figure 10a, the maximum tensile stress in the primary support decreases following a parabolic trend as the offset distance decreases. When the offset distance is 25 m, the maximum tensile stress is 0.29 MPa. As the offset distance is reduced to 20 m and 15 m, the maximum tensile stress increases to 0.32 MPa and 0.41 MPa, corresponding to increments of 10.3% and 31.0%, respectively. When the offset distance is further reduced to 10 m and 5 m, the maximum tensile stress rises sharply to 0.62 MPa and 0.86 MPa, with corresponding increases of 72.4% and 82.8%.

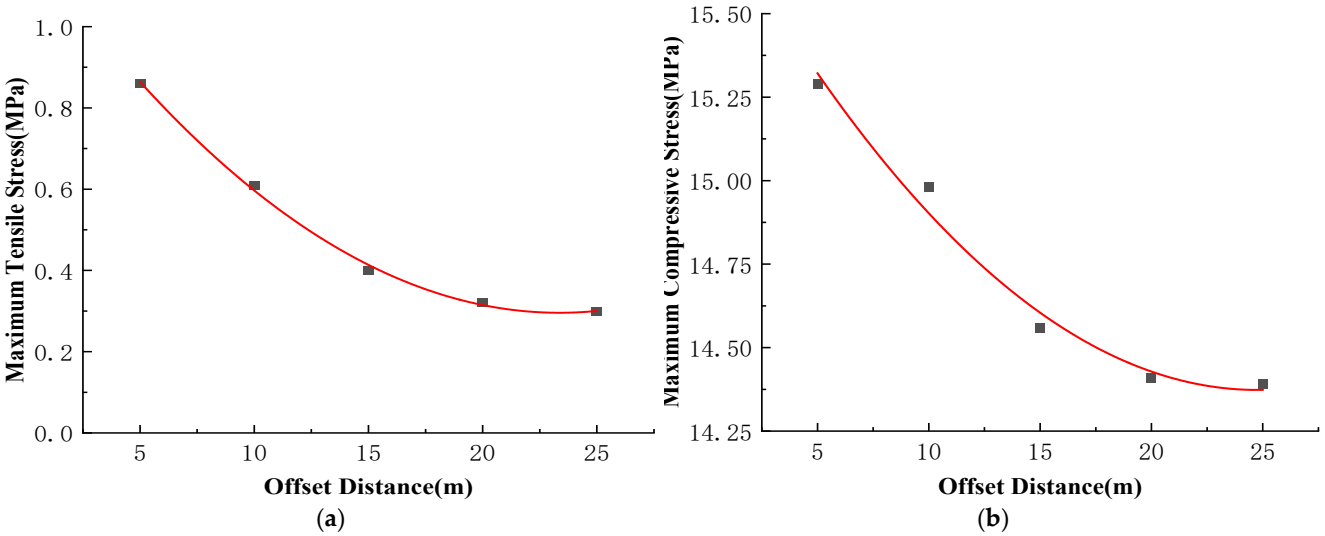

Figure 10. Stress changes in primary support with different offsets ((**a**) Maximum Tensile Stress of Primary Support; (**b**) Maximum Compressive Stress of Primary Support).

As shown in Figure 10b, the maximum compressive stress in the primary support exhibits a parabolic increase with decreasing offset distance. When the offset distance is 25 m, the maximum compressive stress is 14.39 MPa. As the offset distance decreases to 20 m and 15 m, the maximum compressive stress increases by 0.02 MPa and 0.15 MPa, corresponding to increments of 0.1% and 1.1%, respectively. When the offset distance is further reduced to 10 m and 5 m, the maximum compressive stress rises rapidly to 0.35 MPa and 0.38 MPa, with increments of 2.4% and 2.6%, respectively.

4.2.3. Development of Plastic Zone

Figure 11 shows the distribution of the overall plastic zones in the surrounding rock under different offset distances. Analysis indicates that as the offset distance decreases, the area of the plastic zones at the tunnel haunches gradually increases. When the offset distance is reduced to 10 m and 5 m, the plastic zone areas at the left and right haunches increase sharply. This suggests that reducing the excavation offset enhances disturbance to the surrounding rock, and when the offset distance is too small, the plastic zones expand rapidly, which is detrimental to the stability of the tunnel support.

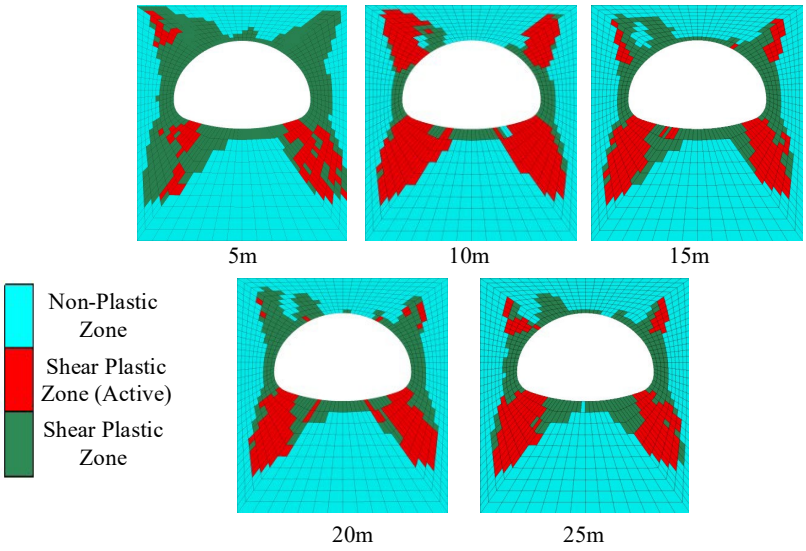

Figure 11. Distribution diagram of plastic zone.

In summary, as the offset distance decreases, the deformation of the tunnel primary support gradually decreases, while both the stress in the primary support and the area of the surrounding rock plastic zones progressively increase. When the offset distance is reduced from 25 m to 15 m, the increases in primary support deformation and plastic zone area are relatively small. However, when the offset distance falls below 15 m, the stress in the primary support and the plastic zone area rise sharply. Therefore, it is recommended that the offset distance in practical engineering should not be less than 15 m.

5. Analysis of On-Site Monitoring and Measurement

5.1. Monitoring Plan/Monitoring Scheme

Based on the results of the previous study, an offset distance of 15 m between the drift faces was selected for on-site excavation. To investigate the actual construction performance of the Double Side Drift Method (DSDM) in mudstone soft rock and the deformation characteristics of the primary support, a test section was established in the field between chainage ZK13 + 400 and ZK13 + 460. A monitoring section was set up at ZK13 + 412 with a burial depth of 15 m to conduct field monitoring of the deformations of both the primary support and temporary support.

At the monitoring section, measurement points were installed at the corresponding locations of the support immediately after each excavation segment and completion of primary support installation (for example, after excavation of Part ① and installation of the primary support, monitoring points A, B, and D were immediately installed at the corresponding positions of the primary support). The positions of the monitoring points were recorded once daily using a total station. The layout of the deformation monitoring points at the section is shown in Figure 12.

5.2. Data Analysis of Primary Support Deformation Monitoring

Figure 13 presents the monitoring results of the tunnel crown settlement and horizontal convergence of the primary support. The crown settlement in each drift increased rapidly within 20 days after the upper bench excavation. With the subsequent excavation, the settlement continued to grow slowly and gradually stabilized after approximately 90 days, when the primary support formed a closed ring. Upon completion of the tunnel excavation, the left drift exhibited the largest cumulative settlement of 30.2 mm, which is 1.8 mm greater than the numerical simulation result. The cumulative settlements of the middle and right

drifts were relatively smaller, 23.7 mm and 25.7 mm, respectively, exceeding the numerical predictions by 3.2 mm and 3.5 mm. The settlement growth rate in the left drift increased again after the excavation of the middle drift upper bench (Section ⑤), and gradually leveled off prior to the removal of the temporary support. The settlement development in the right and middle drifts showed similar patterns, with their secondary increases occurring during the middle drift upper bench excavation and middle drift lower bench excavation, respectively, followed by stabilization before the removal of the temporary support. These observations are generally consistent with the crown settlement evolution obtained from the numerical simulation.

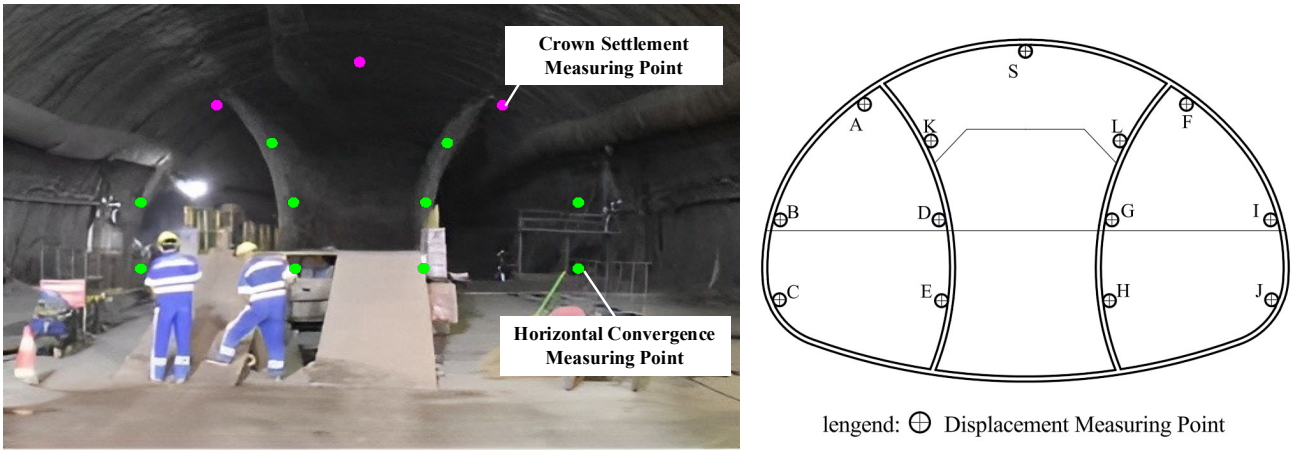

Figure 12. Schematic diagram of on-site displacement measuring point layout for DSDM.

The horizontal convergence in each drift increased rapidly within 15 days after the corresponding excavation stage and then continued to grow slowly during subsequent construction, gradually stabilizing after approximately 100 days of monitoring. This is generally consistent with the horizontal convergence trend obtained from the numerical simulation. Before the removal of the temporary support, the left and right drifts converged inward, with cumulative convergence of 31.7 mm and 27.6 mm at the upper bench, which are 0.1 mm and 0.9 mm smaller than the simulated values, respectively. The lower bench convergence was slightly smaller than that of the upper bench, reaching 27.9 mm and 22.7 mm, which are 4.3 mm and 4.4 mm larger than the numerical results. The middle drift expanded outward, with a cumulative expansion of 23.7 mm, 6.1 mm less than the numerical prediction. After the completion of the overall tunnel excavation, the primary support exhibited overall inward convergence, reaching 35.6 mm, which is 5.1 mm greater than the numerical calculation result.

Based on the above analysis, the deformation obtained from the numerical simulation exhibits slight discrepancies compared with the field monitoring results. The main reasons for these differences are that the geological conditions continuously change during actual construction, the installation timing of the support structures in the field differs from that assumed in the numerical model, and certain measurement errors may occur during the monitoring process. Nevertheless, the deformation patterns of the primary support observed in both the numerical simulation and the actual construction are generally consistent, which fully verifies the reliability of the numerical simulation results presented in this study.

The field-monitored crown settlement and horizontal convergence of the primary support were both below the controlled deformation limits described in Section 2.1, indicating that the design and construction requirements were satisfactorily met. Furthermore,

the trends observed in the field monitoring were generally consistent with the numerical simulation results.

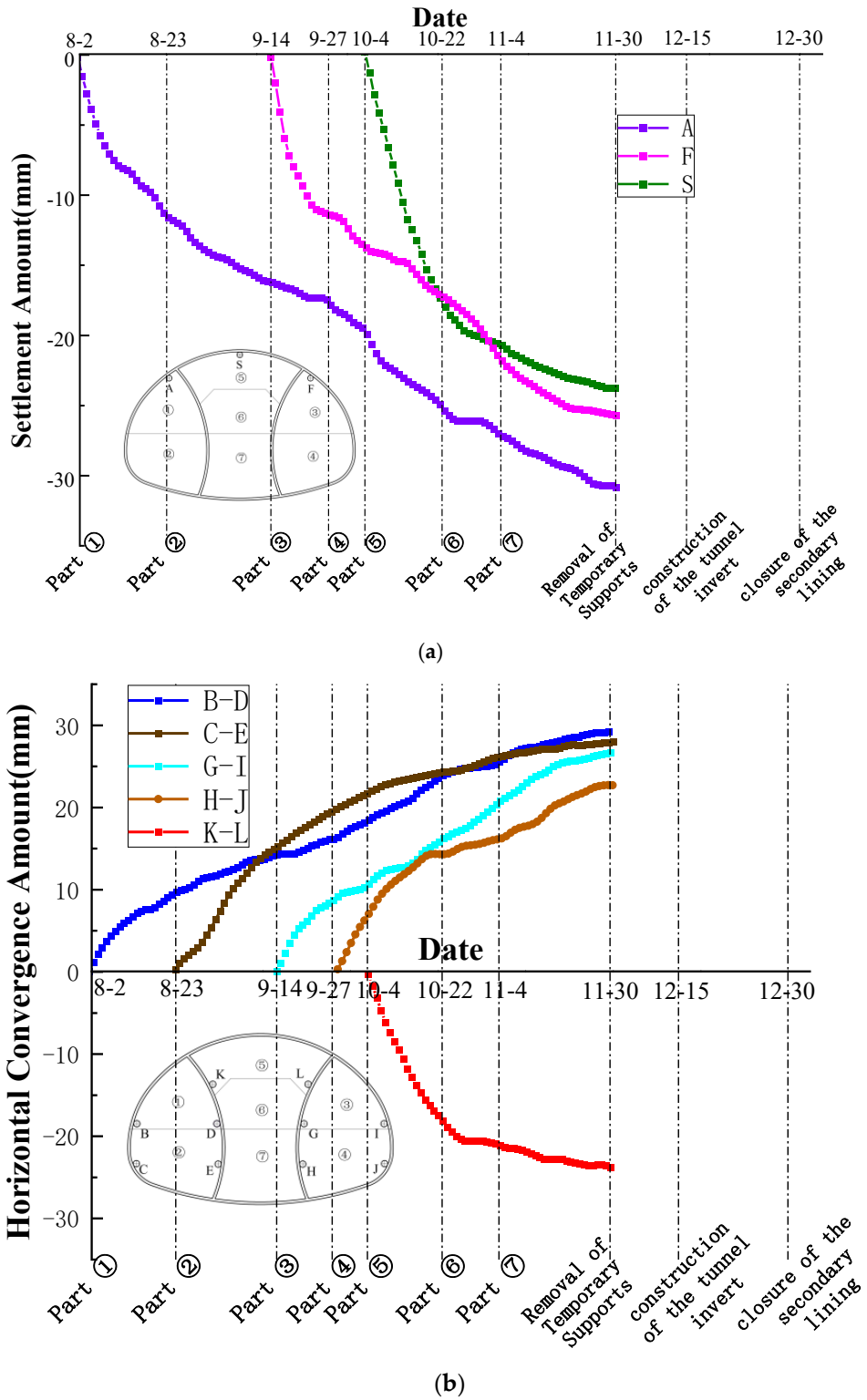

Figure 13. Tunnel deformation monitoring ((**a**) Crown Settlement Curves of Each Drift; (**b**) Horizontal Convergence Curves of Each Drift).

6. Conclusions

This study investigated the mechanical characteristics of a large-span argillaceous soft rock tunnel constructed using the Double Side Drift Method (DSDM), and analyzed the

effects of drift face offset distance on the primary support deformation, stress distribution, and surrounding rock plastic zones. Field monitoring was conducted to ascertain the deformation patterns. The main findings are summarized as follows:

(1) Deformation behavior of the primary support: During DSDM construction, crown settlements of the primary support increase rapidly after excavation of the upper benches and then gradually stabilize. The left drift exhibits the largest settlement, while the central drift shows the smallest. Horizontal convergence follows a similar trend, with the left and right drifts converging inward and the central drift expanding outward. Upper bench excavation induces slightly larger convergence than lower benches, with the left drift upper bench showing the maximum inward convergence.

(2) Stress evolution of the primary support and development of the plastic zone in the surrounding rock: Primary support stresses increase sharply after excavation of each segment and then tend to stabilize. The maximum tensile stress occurs at the left haunch (0.41 MPa), and the maximum compressive stress at the left arch waist (14.56 MPa). After overall excavation, the left side experiences significantly higher stress, resulting in an eccentric stress state. The surrounding rock plastic zones exhibit a butterfly-shaped distribution, concentrated mainly at the haunches and arch springings.

(3) As the drift face offset distance decreases, primary support deformation reduces, while both stress and plastic zone area increase. When the offset distance is less than 15 m, these increases become pronounced, indicating that the drift face offset distance should not be less than 15 m in practice.

(4) Field monitoring confirms that upper bench excavation of each drift has the most significant impact on crown settlement and horizontal convergence. Subsequent excavation induces slow growth in deformation, which eventually stabilizes. The maximum cumulative crown settlement and horizontal convergence at the monitored section are 30.2 mm and 35.6 mm, respectively, both below the reserved deformation allowance.

Author Contributions: Conceptualization, W.H.; methodology, T.W., Y.Z. and F.W.; Software, T.W.; Validation, T.W. and F.W.; Formal analysis, T.W.; Investigation, T.W. and Y.Z.; Resources, F.W.; Data curation, Y.Z.; Visualization, T.W.; Supervision, T.W. and Y.Z.; Project administration, W.H. and F.W. All authors have read and agreed to the published version of the manuscript.

Funding: This research received no external funding.

Data Availability Statement: The original contributions presented in this study are included in the article Further inquiries can be directed to the corresponding author.

Conflicts of Interest: Author Wei He is employed by Hubei Communications Investment Bachu Construction Management Co., Ltd. The other authors declare that this study was conducted without any commercial or financial relationships that could be construed as potential conflicts of interest.

References

1. Wang, M.N.; Guan, B.S.; He, C. Study on mechanical behaviour of three-lane road tunnel under tectonic stresses. *Chin. J. Geotech. Eng.* **1998**, *20*, 51–55.
2. Xia, B.X.; Cheng, C.G. Review on the Research Status of Three-Lane Large-Section Highway Tunnels. *Chin. J. Undergr. Space Eng.* **2002**, *22*, 360–366, 373.
3. Zhang, T. Analysis of mechanical response of four-lane small clear spacing highway tunnel with super-large cross-section. *China Civ. Eng. J.* **2015**, *48* (Suppl. 1), 302–305.
4. Luo, Y.; Chen, J.; Shi, Z.; Li, J.; Liu, W. Mechanical Characteristics of Primary Support of Large Span Loess Highway Tunnel: A Case Study in Shaanxi Province, Loess Plateau, NW China Primary. *Tunn. Undergr. Space Technol.* **2020**, *104*, 103532. [CrossRef]

5. Luo, Y.; Shi, Z.; Chen, J.; Liu, W.; Li, Y.; Wu, Y.; Zhu, H. Study of Deformation Behaviors and Mechanical Properties of Central Diaphragm in a Large-Span Loess Tunnel by the Upper Bench CD Method. *Adv. Civ. Eng.* **2020**, *2020*, 8887040. [CrossRef]
6. Zhou, Z.; Zhao, J.; Tan, Z.; Zhou, X. Mechanical Responses in the Construction Process of Super-Large Cross-Section Tunnel: A Case Study of Gongbei Tunnel. *Tunn. Undergr. Space Technol.* **2021**, *115*, 104044. [CrossRef]
7. Shen, Y.B.; Yang, C.; Wang, Q.; Zhao, Y.W. Spatio-temporal Effect of Long-span Loess Tunnel Surrounding Rock Deformation. *J. Highw. Transp. Res. Dev.* **2024**, *41*, 190–197.
8. Lei, Y.F.; Shi, C.H. Study on deformation control technology of shallow and large cross-section tunnel beneath expressway in soft rock. *J. Railw. Sci. Eng.* **2018**, *15*, 1239–1246.
9. Li, J.; Tan, Z.S.; Yu, Y.; Ni, L.S. Research on construction procedure for shallow large-span tunnel undercrossing highway. *Rock Soil Mech.* **2011**, *32*, 2803–2809.
10. Tian, C.; Chen, J.; Luo, Y.; Liu, W.; Li, Y.; Zhang, L.; Gao, B.; Li, J. Ground Movement Induced by Tunnelling in Shallow Loess Strata. *Tunn. Undergr. Space Technol.* **2026**, *168*, 107156. [CrossRef]
11. Zhao, Y.; He, H.; Li, P. Key Techniques for the Construction of High-Speed Railway Large-Section Loess Tunnels. *Engineering* **2018**, *4*, 254–259. [CrossRef]
12. Ma, L.; Dai, J.; Wang, B.; Mo, Y.; Liu, Y.; Tian, C. Structural Analysis of Large-Span Tunnel Excavated by Upper Bench Center Diaphragm Method: An Analytical Model and Its Application. *Tunn. Undergr. Space Technol.* **2026**, *167*, 107053.
13. An, Z.; Ma, W.; Wang, Y.; Yuan, Z. Stability Analysis of Extra-Large-Span Tunnels During Construction: A Case Study. *Geotech. Geol. Eng.* **2024**, *42*, 3107–3121.3495. [CrossRef]
14. Luo, Y.; Chen, J.; Shi, Z.; Zhang, S.; Liu, W.; Li, Y.; Chen, L. Performance of Super-Large-Span Tunnel Portal Excavated by Upper Bench CD Method Based on Field Monitoring and Numerical Modeling. *Adv. Civ. Eng.* **2020**, *2020*, 8824618. [CrossRef]
15. Li, L.; Shang, C.; Chu, K.; Zhou, Z.; Song, S.; Liu, Z.; Chen, Y. Large-Scale Geo-Mechanical Model Tests for Stability Assessment of Super-Large Cross-Section Tunnel. *Tunn. Undergr. Space Technol.* **2021**, *109*, 103756. [CrossRef]
16. He, J.; He, S.; Liu, X.; Ma, J.; Li, Y.; Zhang, B. Investigating the Mechanical Responses and Construction Optimization for Shallow Super-Large Span Tunnels in Weathered Tuff Stratum Based on Field Monitoring and Flac3D Modeling. *Int. J. Civ. Eng.* **2024**, *22*, 379–395. [CrossRef]
17. Tu, H.; Zhou, H.; Qiao, C.; Gao, Y. Excavation and Kinematic Analysis of a Shallow Large-Span Tunnel in an up-Soft/Low-Hard Rock Stratum. *Tunn. Undergr. Space Technol.* **2020**, *97*, 103245. [CrossRef]
18. Zhou, D.; Cao, L.; Ma, Y.; Fang, S.; Wang, K. Research on construction behaviors of support system in four-lane ultra large-span tunnel with super-large cross-section. *Chin. J. Rock Mech. Eng.* **2010**, *29*, 140–148.
19. Shi, Y.; Li, J.; Li, W.; Zhou, X. Construction mechanics of tunnel with super-large cross-section and its dynamic stability. *J. Shanghai Jiaotong Univ.* **2015**, *49*, 1023–1029.
20. Liu, C.; Li, S.C.; Zhou, Z.Q.; Li, L.P.; Wang, K.; Hou, F.J.; Qin, C.S.; Gao, C.L. Model test on mechanical characteristics of surrounding rock during construction process of super-large section tunnel in complex strata. *Rock Soil Mech.* **2018**, *39*, 3495–3504.
21. Xu, X.D.; Liu, J.; Duan, Y.F.; Xie, H.W. Excavation Scheme of the Large-span Flat and Super-large Section Tunnel of Lianhuo High-speed Xinghua Village No. 1. *Sci. Technol. Eng.* **2023**, *23*, 12258–12264.
22. Tao, J.Q.; Yang, Y.F.; Gao, H.C.; Zhang, Y.Y.; Wang, F. Study on Construction Method Optimization and Mechanical Characteristics of Super-large Section Soft Rock Tunnel. *Chin. J. Undergr. Space Eng.* **2023**, *19* (Suppl. 2), 819–827.
23. Lin, F.; Tao, J.Q.; Gao, H.C.; Zhang, Y.Y.; Pan, Y.D.; Wang, F. Analysis of Construction Mechanical Characteristics and Construction Method Adaptability of Shallow Super-large Section Tunnel in Argillaceous Soft Rock. *Highway* **2022**, *67*, 388–396.
24. Tan, Q.; Hu, B.; Liu, L.; Cheng, Y.; Sharifzadeh, M.; Nie, M.; Zhang, T.; Guo, W.; Cheng, L. Comparative Analysis of Creep Mechanical Characteristics of Yellow Mudstone Tunnel in Natural and Saturated Conditions: Insights from Experiments and Numerical Modeling. *Eng. Fail. Anal.* **2025**, *182*, 110121. [CrossRef]
25. Jiang, Z.L. Construction Parameters Optimization for Double-sidewalls Guiding-hole Method of Shallow Buried Urban Subway Tunnel in Loess Formation. *Railw. Eng.* **2022**, *62*, 126–131.
26. Wang, X.B. Construction Parameter Optimization of Both Side Heading Method for Super Shallow embedded Tunnel with Large Cross-section Fujian. *Fujian Constr. Sci. Technol.* **2012**, *6*, 78–80.
27. Wang, F.; Zhang, Y.Y.; Tao, J.Q.; Gao, H.C. Research on Construction Parameters of Half-Step CD Method with Side Wall Slotting for Large-Span Soft Rock Tunnels. *Hailw. Stand. Des.* **2025**, *69*, 133–141.
28. *JTG 3370.1*; Specifications for Design of Highway Tunnels Section 1 Civil Engineering. Ministry of Transport of the People's Republic of China: Beijing, China, 2018.
29. Deshpande, S.; Hedaoo, N. Evaluation of Face Stability for Mega Tunnel Under Varying Ground Strength Parameters. *Civ. Environ. Eng.* **2024**, *20*, 720–729. [CrossRef]
30. Pan, R.; Zhou, B.; Jiang, D. Mechanical Response and Stability Optimization of Shallow-Buried Tunnel Excavation Method Conversion Process Based on Numerical Investigation. *Buildings* **2024**, *14*, 1213. [CrossRef]

31. Lei, M.; Zhao, C.; Jia, C.; Shi, C. Study on the Geological Adaptability of the Arch Cover Method for Shallow-Buried Large-Span Metro Stations. *Tunn. Undergr. Space Technol.* **2023**, *132*, 104897. [CrossRef]
32. Xiao, J.Z.; Dai, F.C.; Wei, Y.Q.; Min, H.; Xu, C.; Tu, X.B.; Wang, M.L. Cracking Mechanism of Secondary Lining for a Shallow and Asymmetrically-Loaded Tunnel in Loose Deposits. *Tunn. Undergr. Space Technol.* **2014**, *43*, 232–240. [CrossRef]

Disclaimer/Publisher's Note: The statements, opinions and data contained in all publications are solely those of the individual author(s) and contributor(s) and not of MDPI and/or the editor(s). MDPI and/or the editor(s) disclaim responsibility for any injury to people or property resulting from any ideas, methods, instructions or products referred to in the content.